Monthly Notices
of the
ROYAL ASTRONOMICAL SOCIETY

MNRAS **462,** 3302–3313 (2016)
Advance Access publication 2016 July 25

doi:10.1093/mnras/stw1772

BPASS predictions for binary black hole mergers

J. J. Eldridge[1]★ and E. R. Stanway[2]★

[1]*Department of Physics, University of Auckland, Private Bag 92019, Auckland, New Zealand*
[2]*Department of Physics, University of Warwick, Gibbet Hill Road, Coventry CV4 7AL, UK*

Accepted 2016 July 18. Received 2016 July 14; in original form 2016 February 17

ABSTRACT

Using the Binary Population and Spectral Synthesis code, BPASS, we have calculated the rates, time-scales and mass distributions for binary black hole (BH) mergers as a function of metallicity. We consider these in the context of the recently reported first Laser Interferometer Gravitational-Wave Observatory (LIGO) event detection. We find that the event has a very low probability of arising from a stellar population with initial metallicity mass fraction above $Z = 0.010$ ($Z \gtrsim 0.5\,Z_{\odot}$). Binary BH merger events with the reported masses are most likely in populations below 0.008 ($Z \lesssim 0.4\,Z_{\odot}$). Events of this kind can occur at all stellar population ages from 3 Myr up to the age of the Universe, but constitute only 0.1–0.4 per cent of binary BH mergers between metallicities of $Z = 0.001$ and 0.008. However at metallicity $Z = 10^{-4}$, 26 per cent of binary BH mergers would be expected to have the reported masses. At this metallicity, the progenitor merger times can be close to $\approx$10 Gyr and rotationally mixed stars evolving through quasi-homogeneous evolution, due to mass transfer in a binary, dominate the rate. The masses inferred for the BHs in the binary progenitor of GW 150914 are amongst the most massive expected at anything but the lowest metallicities in our models. We discuss the implications of our analysis for the electromagnetic follow-up of future LIGO event detections.

Key words: gravitational lensing: micro – gravitational waves – binaries: general – stars: evolution.

1 INTRODUCTION

The recent detection of a gravitational wave transient from the inspiral of a binary black hole system (BH-BH; Abbott et al. 2016a) opens a new era in observations of the Universe. While the existence of gravitational waves had been inferred from observations of binary pulsar systems (Hulse & Taylor 1975), for the first time, ground-based, laser interferometric experiments have made it possible to observe a BH-BH merger and infer its parameters independently of electromagnetic observations.

The detection of a gravitational wave transient, GW 150914, by the Laser Interferometer Gravitational-Wave Observatory (LIGO; LIGO Scientific Collaboration et al. 2015) was reported on 2016 Feb 11. Detected on 2015 September 14, during the first advanced-LIGO operational run, the transient's characteristics are consistent with the inspiral, merger and ring-down of a binary system comprising two BHs, with estimated masses of 36^{+5}_{-4} and 29^{+4}_{-4} $M_{\odot}$ (Abbott et al. 2016b). This event constitutes the first detection of gravitational wave emission, and is notable in that it represents a BH-BH merger, rather than the neutron star–neutron star (NS-NS) mergers expected to be more common (if less luminous) sources at LIGO frequencies and sensitivities (e.g. Abadie et al. 2010; Berry et al. 2015), although it was predicted by some that BH-BH mergers would be more likely (Belczynski et al. 2010; Dominik et al. 2015). The event was not securely localized in electromagnetic follow-up (although see Connaughton et al. 2016), and hence its host galaxy, and the stellar population that generated it, remains unidentified.

Nearly all the BHs in the Universe are thought to be the end result of stellar evolution. The only other source may be primordial BHs formed during the big bang; these would only occur if density perturbations are great enough that gravitational collapse would occur during the early Universe (Carr 2003). Massive stars with initial masses $\gtrsim$20 $M_{\odot}$ create sufficiently massive cores at the end of their luminous lifetimes that they cannot avoid collapse to BHs under self-gravity, although stars with masses above $\gtrsim$100 $M_{\odot}$ at low metallicities may undergo pair-instability supernovae (SNe) and leave no remnant (e.g. Heger & Woosley 2002). Massive stars that are below $\sim$20 $M_{\odot}$ or those that experience a binary interaction instead collapse to a neutron star remnant. This neutron star may then collapse into a BH as a result of mass transfer from a binary companion. Predicting the rates of formation and merger of BH systems thus requires stellar population synthesis: the process by which stellar evolution models are combined and weighted according to an initial mass function (IMF). Such models have a long history (e.g. Tutukov & Yungelson 1973; Tinsley & Gunn 1976).

Today there is growing evidence that most massive stars are in binary or multiple systems, with 70 per cent of massive stars having their evolution affected by binary interactions as shown by

★ E-mail: j.eldridge@auckland.ac.nz (JJE); e.r.stanway@warwick.ac.uk (ERS)

direct and indirect observations (e.g. Vanbeveren, De Loore & Van Rensbergen 1998; Eldridge, Izzard & Tout 2008; Sana et al. 2012, 2014). The presence of a nearby stellar companion can cause a star to experience very different evolutionary pathways to those of isolated stars. In general these complicate stellar evolution, allowing extra opportunities for mass-loss and mass gain.

There are several mature binary population synthesis codes world-wide (e.g. Vanbeveren et al. 1998; Hurley, Tout & Pols 2002; Izzard, Ramirez-Ruiz & Tout 2004; Lipunov & Pruzhinskaya 2014; Mennekens & Vanbeveren 2016). Most have been used to make predictions for the merger rates of compact objects and the mass range for such mergers (e.g. Bogomazov, Lipunov & Tutukov 2007; Lipunov & Pruzhinskaya 2014; de Mink & Belczynski 2015; Kowalska-Leszczynska et al. 2015; Belczynski et al. 2016b; Mandel 2016; Mandel & de Mink 2016). With the detection of GW 150914 we now have a first observational datum to compare against such models; a situation analogous to the first detection of a SN progenitor star (that of SN 1987A, now known to be a rare progenitor type) in pre-explosion imaging which provided an immediate constraint on stellar models (Walborn et al. 1987; Podsiadlowski 1992). While we should exercise caution, since GW 150914 may prove similarly atypical of its population, it is none the less useful to analyse the detection in the light of theory.

In this paper, we calculate the expected rate and parameters for BH-BH mergers from our Binary Population and Spectral Synthesis code, BPASS v2.0 models, and how these vary with initial metallicity of the stellar population. In Section 2, we describe the BPASS stellar population synthesis code and the numerical method employed in this analysis. In Section 3, we present rates and time-scales for binary BH mergers. We also identify a metallicity cut-off, indicating that the progenitor system likely formed in a low-metallicity environment, as predicted by Belczynski et al. (2010). In Section 4 we show that, at low metallicities, the rate of BH mergers peak for BH binaries with near equal mass objects, similar to the reported mass ratio of the progenitors of GW 150914. Finally, in Section 5 we discuss the implications for searching for electromagnetic counterparts of such events, before presenting our conclusions in Section 6.

2 NUMERICAL METHOD

2.1 BPASS description and initial parameters

The BPASS, code was first discussed in Eldridge et al. (2008), which also outlines modifications to the Cambridge STARS code used to create the stellar evolution models. A key difference between BPASS and most other codes is our use of a large grid of 250 000 stellar models to follow the evolution of interacting binary stars (e.g. Vanbeveren et al. 1998), rather than using the approximation methods employed by rapid population synthesis codes (e.g. Hurley et al. 2002). The rapid method allows for the uncertainties of binary evolution and their impact on predictions to be explored; this would be too computationally intensive for detailed stellar models. The use of detailed models, on the other hand, allow us to accurately follow how the stellar envelope responds to mass-loss – key to determining the eventual mass and fate of the star. The spectral synthesis of stellar populations from individual stellar models was described in Eldridge & Stanway (2009, 2012), while a study of the effect of SN kicks on the stellar populations and SNe was described in Eldridge, Langer & Tout (2011). Many of the results for the code are available at http://bpass.auckland.ac.nz.

BPASS models have been tested by the authors and others against resolved and unresolved massive stellar populations in our Galaxy, nearby galaxies and those at high redshift (e.g. Eldridge et al. 2008, 2011; Eldridge & Stanway 2009, 2012; Stanway et al. 2014). They have also been tested against directly detected SN progenitors and relative SN rates (e.g. Eldridge et al. 2013, 2015; Xiao & Eldridge 2015). Furthermore we have recently released version 2.0 of BPASS (Stanway, Eldridge & Becker 2016, Eldridge et al., in preparation). This incorporates many refinements to the code and its outputs compared to the earlier versions. The results of BPASS v2.0 have already further demonstrated the improvement in agreement between observations and stellar population models that arises from the inclusion of interacting binaries (e.g. Ma et al. 2016; Stanway et al. 2016; Wilkins et al. 2016; Wofford et al. 2016).

While BPASS has been described in detail previously we provide a detailed summary of BPASS here for those unacquainted with the code. We use an IMF based on Kroupa, Tout & Gilmore (1993), with a power-law slope of -1.3 between initial masses of 0.1 and 0.5 $M_\odot$ and a slope of -2.35 from 0.5 to 300 $M_\odot$. The stellar mass function therefore dictates that less massive stars are more numerous and therefore fewer massive remnants and BHs are generated than in a standard, unbroken Salpeter IMF. This is combined with an initial-mass ratio of M_2/M_1 that is uniformly distributed between 0 and 1. All secondary stars contribute to the stellar mass but we do not include a companion in the total stellar mass estimate if its initial mass is less than 0.1 $M_\odot$.

Key refinements in BPASS v2.0 (relative to the v1.1 models discussed in Eldridge et al. 2008, 2011; Eldridge & Stanway 2009, 2012) that affect the results of this paper are as follows. First, we increase the number of models we have for our entire population from 15 000 detailed stellar evolution models to 250 000 which represents several years of computational time if run on a single processor. This increase allows us to sample the initial parameter space for our initial masses at a greater resolution. We have a grid of 68 initial primary masses from $M_1 = 0.1$ to 300 $M_\odot$, nine values for the mass ratio, q, from $M_2/M_1 = 0.1$ to 0.9 and 21 initial periods from 1 d to 10 000 d. We also increase our grid of initial metallicities to $Z = 0.000\,01$, 0.0001, 0.001, 0.002, 0.003, 0.004, 0.006, 0.008, 0.010, 0.014, 0.020, 0.030 and 0.040.

The initial period distribution is uniformly distributed in logarithm of the period from 1 to 10^4 d. We note that by observing O stars in the Galaxy, Sana et al. (2012) found that the observed period distribution is somewhat steeper with a bias towards more close binary systems. However Kiminki & Kobulnicky (2012) found a flatter period distribution in the Cygnus OB2 association that is consistent with Opik's law, although their results did also suggest a slight preference for short period systems. The uncertainty in assumed period distribution is degenerate with uncertainties in the assumed model to handle Roche lobe overflow, common-envelope evolution, tides and other binary specific processes. Furthermore it is unknown whether the observed period distributions should be extended to all stellar masses. We can gain some insight into the effect of how varying the initial period distribution will affect our results by looking at the work of de Mink & Belczynski (2015), who find that the rates of gravitational wave events will increase by a factor of 2 if a distribution favouring short periods is used. Therefore we can say that any predictions for our code are most likely a lower estimate on the possible rate.

We assume orbits are circular, or rather that the semilatus rectum distribution is flat. This can be assumed because, as shown by Hurley et al. (2002), the outcome of the interactions of systems with the same semilatus rectum is almost independent of eccentricity. This is also equivalent of assuming that systems are circularized before interactions by tides. We only include tides in our evolution models

when a star fills its Roche lobe. Then we assume tidal forces are strong and the star's rotation quickly synchronizes with the orbit. This is of course approximate and there are recent studies have begun to explore how mass transfer may be different in eccentric systems (Bobrick, Davies & Church 2015; Dosopoulou & Kalogera 2016a,b). However, we note that the BPASS models have been tested to see if they can reproduce an observed binary system with a slight eccentricity even after mass transfer (Eldridge 2009).

We scale the mass-loss rates applied from those observed in the local Universe, such that $\dot{M}(Z) = \dot{M}(Z_{\odot})(Z/Z_{\odot})^{\alpha}$ and $\alpha = 0.5$ (except in the case of OB stars where $\alpha = 0.69$; see Vink, de Koter & Lamers 2001). There is little consensus in the literature regarding the definition of solar metallicity. Villante et al. (2014), for example, suggest that the metal fraction in the Sun is rather higher than usually assumed, while some authors (Allende Prieto, Lambert & Asplund 2002; Asplund 2005) suggest that solar metal abundances should be revised downwards to closer to $Z = 0.014$ (also appropriate for massive stars within 500pc of the Sun, Nieva & Przybilla 2012). We retain $Z_{\odot} = 0.02$ for consistency with the empirical mass-loss rates which were originally scaled from this value. We note that at the lowest metallicities of our models the small uncertainty in where we scale the mass-loss rates will cause only small changes in the mass-loss rates due to stellar winds. At the lowest metallicities, mass-loss is primarily driven by binary interactions.

A key feature of the BPASS models that sets them apart from others, except the Brussels code (Vanbeveren et al. 1998; Mennekens & Vanbeveren 2016), is that all the interacting binary evolution models are evolved in a full detailed stellar evolution code that is based on the Cambridge STARS code and described in detail in Eldridge et al. (2008). This greatly increases our computational needs with the stellar models each taking several minutes to calculate rather than fractions of a second. The v2.0 models in this paper represent a total computing time on a single computer of over five years. However while we have a computational cost and therefore have to make assumptions, such as circular orbits, we have significant gain in the accuracy of the stellar evolution models. We find differences in how the stellar envelope responds to mass-loss relative to rapid population synthesis, as discussed in Eldridge et al. (2008). A comparison between our models and those of a rapid population synthesis code show that our models would explode as red or yellow supergiants while a rapid code assumed they would become Wolf–Rayet stars.

We note we only compute one star in detail at a time. This is because stars of very different masses have different evolutionary time-scales. Therefore computational time would be wasted on calculating the evolution of a 1 $M_{\odot}$ secondary star at the same time as a 10 $M_{\odot}$ primary. We therefore calculate the primary evolution first, using the single-star rapid evolution equations of Hurley et al. (2002) to approximate the secondary's evolution. We then recalculate the secondary's evolution in the same detailed code either as a single star or in a binary with a compact remnant depending on whether the binary is bound or unbound. We also do not interpolate between these detailed models due to the non-linear nature of binary evolution. The entire scheme is discussed in greater detail in Eldridge et al. (2008) and Eldridge et al. (2011).

One further refinement is vital for this work, that is the treatment of the secondary models. In most SNe, a binary is unbound in the first SN and thus the secondary evolves afterwards as a single star. However in the case of those that remain bound BPASS selects from a grid of binary models where the secondary is a compact remnant to represent the further evolution of what was originally the secondary star. Due to computational constraints in Eldridge et al. (2008) we only assumed three masses for compact remnants, 0.6, 1.4 and 3 $M_{\odot}$ for white dwarfs, neutron stars and BHs. In BPASS v2.0 we now calculate the full range of possible secondary evolution in binaries, allowing for a range of masses for the compact remnant from 0.1 to 300 $M_{\odot}$. We stress that this is different to rapid codes that would typically take the evolutionary outcome of the secondary and continue to evolve it. Due to our use of detailed stellar evolution models this is still not computationally feasible. Our extended selection of secondary models allow us to follow evolution up to the formation of massive double BH binaries.

We follow the evolution and include mass transfer when a star fills its Roche lobe, full details are given Eldridge et al. (2008). We assume any mass lost from the primary is transferred to the secondary but this can only be accreted by the secondary on a thermal time-scale, any extra mass is lost from the system. If the star filling its Roche lobe engulfs the other star we assume common-envelope evolution occurs. In a detailed stellar evolution code, we cannot simply remove the stellar envelope instantaneously (as described in Eldridge et al. 2008). Instead we increase the mass-loss rate to as high as numerically possible. Then at each timestep we calculate the binding energy of material lost in our common-envelope wind and remove this from the orbital energy of the star's core and the secondary star. If the secondary star fills its Roche lobe, we merge the two stars together. This is, of course, approximate and different to the typical implementation in other models but a reasonable approximation. It is likely to be one of the sources of differences between our models and those of others. A consequence of our method is that it is not straightforward to vary the physics of binary interactions, since this would require recalculation of the entire model set. While we do explore some key parameters, such as IMF, with different model grids, we do not vary others, such as those controlling common-envelope evolution.

2.2 Quasi-homogeneous evolution

Our models only account for rotationally induced mixing in a simple way. We assume that if a secondary star in one of our models accretes more than 5 per cent of its initial mass and it is more massive than 2 $M_{\odot}$ then the star is spun-up to critical rotation and is rejuvenated due to strong rotational mixing. That is, it evolves from the time of mass transfer as a zero-age main sequence star (this is similar to the method used by Vanbeveren et al. 1998). At high metallicities, we assume that the star quickly spins down by losing angular momentum in its wind so that there are no further consequences to evolution. However with weaker winds at lower metallicity, $Z \leq 0.004$, we assume that the spin-down occurs less rapidly and so the star is fully mixed on the main sequence and burns all its hydrogen to helium. We assume that the star must have an effective initial mass after accretion >20 $M_{\odot}$ for this evolution to occur. These limits were taken from the work of Yoon, Langer & Norman (2006). We note that we have discussed the importance of these quasi-homogeneously evolving (QHE) stars in greater detail in Eldridge et al. (2011); Eldridge & Stanway (2012) and Stanway et al. (2016) showing there is strong observational evidence they exist. The key difference we find from QHE changing the formation of BH-BH binaries in our models is that it greatly increases the chance that the second BH to form is the more massive remnant. Because a QHE star never evolves to the red supergiant (RSG) phase, the mass-loss it experiences is less and more of the mass accreted by the secondary is retained during the star's evolution.

Furthermore our QHE is the result of mass transfer only. Mandel & de Mink (2016) and Marchant et al. (2016) invoke a different mechanism to create QHE stars. They consider the closest binaries

with the shortest rotation periods, of the order of a day, so that both stars experience QHE with the rapid rotation induced due to tidal interactions between the stars. While this is a very plausible pathway, we have not yet included this in our standard BPASS evolution models. Here we concentrate on the mass transfer pathway to QHE. The rates we predict here might still be further boosted if we were to include such additional pathways. At the current time in our population the binaries in Mandel & de Mink (2016) and Marchant et al. (2016) are likely to result in mergers or Roche lobe overflow because we do not assume those stars experience QHE due to tidal forces.

Finally, we note that we assume that QHE is due to rotational mixing and it is different from the type of chemically homogeneous evolution found in models of very massive stars, $\gtrsim$150 $M_\odot$. Yusof et al. (2013) find such stars have very large convective cores so that mass-loss can expose material from the core rapidly without the need for rotational mixing.

2.3 Predicting the remnant masses and SN kick velocities

To estimate remnant masses our stellar models produce, we use the method described in Eldridge & Tout (2004). We calculate how the binding energy of the star varies with stellar radius. We assign as ejecta all material that is above the point where the binding energy is equal to 10^{51} erg. We assume a BH is formed when the remnant mass is above 3 $M_\odot$, otherwise we assume a neutron star forms with a mass of 1.4 $M_\odot$. While this method is approximate, it does give a reasonable estimate for the size of the remnant and agrees with other predictions for the initial masses when neutron stars or BHs are formed during core collapse (e.g. Heger et al. 2003; Ugliano et al. 2012; Spera, Mapelli & Bressan 2015; Sukhbold et al. 2016). We note that the link between final remnant mass and initial mass can be highly non-linear. For example, stars above $\approx$20 $M_\odot$ form BHs, while stars below form neutron stars. However at higher initial masses, mass-loss can still lead to the formation of neutron stars (e.g. Heger et al. 2003; Eldridge & Tout 2004; Ugliano et al. 2012; Sukhbold et al. 2016). We do not include remnants from stars that end their evolution with helium core masses between 64 and 133 $M_\odot$ which are thought to explode in pair-instability SNe and leave no remnant (Heger & Woosley 2002).

Once the remnant and its mass is determined we use the kick distribution of Hobbs et al. (2005) to pick a kick velocity and direction at random. For BH kicks, we assume a momentum distribution and reduce the kick velocity by multiplying it by 1.4 $M_\odot$ and dividing by the BH mass. We do this because of the growing evidence as discussed by Mandel (2016) that BH kicks are smaller than those of neutron stars. The full method of determining kicks and the fate of the binary when a SN occurs within it are described in Eldridge et al. (2011).

To provide some test of the accuracy of this estimation we have compared our predicted BH masses to those observed in nature in Fig. 1. We see that the BH masses predicted by our single-star and binary star populations are similar and agree with the increasing trend of BH masses with metallicity from the results of Crowther et al. (2010). There have also been some suggestions that there is a gap in the BH masses expected from stellar evolution, i.e. that there are no BHs in the mass range between 3 and 5 $M_\odot$ (Belczynski et al. 2012). We see in Fig. 1 that fewer than half of all BHs should have masses in this range in our Galaxy. Also binary systems containing these objects are more likely to become unbound as they will have larger kicks in our population under our assumptions for natal BH kicks. We show in Fig. 1 the mean mass of

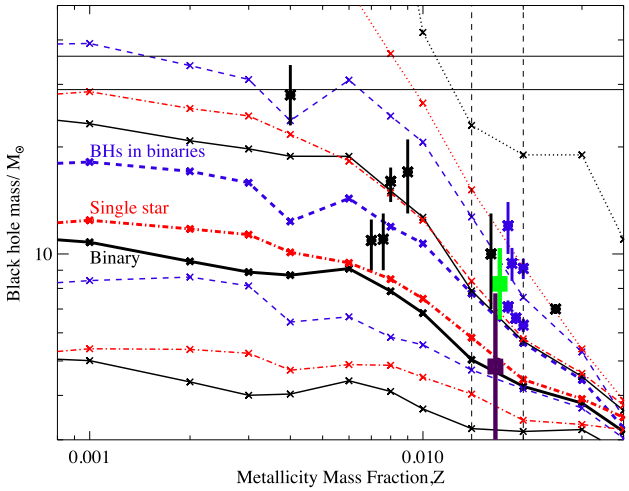

Figure 1. The mean and maximum BH natal masses from our models. The thick lines are the mean BH masses, the thin lines indicate the 1σ ranges, while the dotted line are the maximum BH masses. The red dash-dotted lines are for single-star models and the black solid lines are for our binary models. The blue dashed lines represents the mean mass of BHs that remain in binary systems. The solid thick vertical black lines with asterisks represent the BH masses collated in Crowther et al. (2010). While the blue asterisk and lines represent the Galactic BH masses from Özel et al. (2010). Since the metallicities of Galactic BH progenitors are unconstrained, we show them as lying close to $Z = 0.02$, with small offsets for clarity. Vertical lines indicate two widely used values for solar metallicity. We also plot the mean mass of these Galactic BH binaries in the green or light grey square and the mean mass of the single BH candidates identified from gravitational microlensing by Wyrzykowski et al. (2016) in the purple or dark grey square. The two thin horizontal lines indicate the masses of the BHs from GW150914.

BHs in binary systems. This is higher than the overall mean and the observed BHs do lie closer to this line. Future observing campaigns for mergers involving BHs will show if there are such systems. We note here that we may over predict the BH-BH merger rate at higher metallicities because we include these objects.

Recently Wyrzykowski et al. (2016) have detailed a number of candidate single compact remnants in the Galaxy discovered via gravitational microlensing. They found no evidence for a gap in the mass of remnants between neutron stars and BHs as suggested by Belczynski et al. (2012). We have estimated a mean mass for single/runaway BHs from the sample of Wyrzykowski et al. (2016). We have assumed the same minimum mass for an object to be a BH as in our models of 3 $M_\odot$. The mean is then based on seven objects with the most massive being $9.3^{+8.7}_{-4.3}$ $M_\odot$. There are a further three objects in their sample between 2 and 3 $M_\odot$, including these would reduce to mean to 3.8 $M_\odot$. We see that this mean is close to the mean BH mass predicted at solar metallicity for our model populations. Again the sample is small but future events from gravitational microlensing will increase our understanding of BH formation as much as future gravitational wave sources.

We further note that while the mean BH mass from a binary population is slightly less than that from a single-star population, our models show the maximum mass of a BH is greater from our binary populations. This is because mergers and mass transfer in our models allow stars to regain some of their lost mass from a companion and also to create stars more massive than our assumed 300 $M_\odot$ upper mass limit, although all binary evolution codes include this possibility. Also all codes include the mass of the BHs being able to

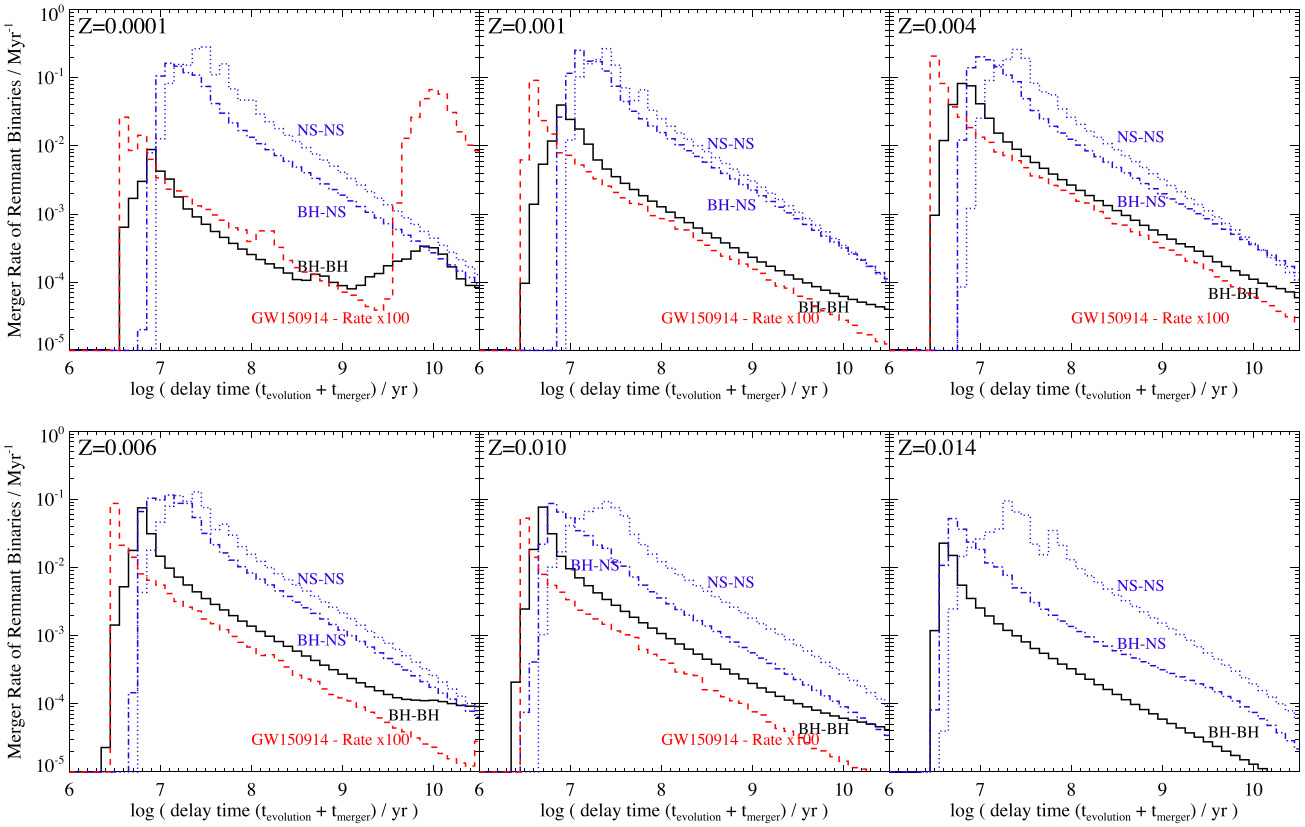

Figure 2. The merger rate of systems with different delay times at various metallicities. They are calculated assuming an instantaneous burst of star formation at $t = 0$ with a total stellar mass of 10^6 M$_\odot$. In all cases, the merger time dominates the delay time but the stellar lifetime does give rise to the minimum total time (∼3 Myr). The thick black line shows the delay time distribution for BH-BH mergers. The red dashed line represent the population of systems matching GW 150914 with the rate boosted by a factor of 100 for visibility. The blue dotted line is the rate for NS-NS binaries and the blue dash–dotted line for NS-BH mergers.

increase via accretion from their companion star Wiktorowicz et al. (e.g. 2015).

We also find that, while Belczynski et al. (2016a) suggest binary interactions only lead to less massive BHs in a population for the specific case of forming close massive BH binaries we find this situation is not that simple. We find that some interacting binaries actually lead to a more massive BH than possible for a star of the same mass from single-star evolution. We find that in some cases a binary interaction during or before first dredge-up (i.e. when the star becomes a red supergiant) in a model can prevent or weaken dredge-up. This leads to a more massive helium core for the stellar model than expected if it was single, and therefore eventually a more massive BH. This increase of the final BH mass is of the order of 10 per cent. We believe this difference is due to our use of a detailed stellar evolution code and thus the ability to follow how the development and extent of convective zones within the stellar interior are affected by a binary interaction. Without this, so subtle an effect might be missed.

2.4 Compact remnant merger time calculation

Our only addition to the BPASS code specifically predict the merger rate of BH binaries has been to use the final orbital parameters after the second SN in the binary system to calculate how long it will take for the two BHs to merge. In common with Mandel & de Mink (2016), we use the analytic form of Peters (1964) to calculate this merger time. Peters gives two limits for the merger time for low- and high-eccentricity orbits. For rapid computation of our population, we interpolate between these two limits linearly. While a full solution for evolution over time might give a more precise solution, the uncertainties introduced by interpolation are smaller than those implicit in the assumptions and uncertainties involved in other aspects of stellar population synthesis.

To calculate the delay time for a BH merger event we calculate an evolution time, $t_{\rm evolution}$, defined as the interval after the onset of star formation required for the progenitor stars to evolve and create the two BHs. We combine these evolution time-scales with the time required for inspiral to calculate a total required delay time, $t_{\rm delay}$. We then use this to calculate a Galactic merger rate by assuming a constant star formation rate of 3.5 M$_\odot$ yr^{-1} for 10 Gyr, i.e. we predict the number of BH binary mergers expected per year if the Milky Way was made gradually, of stars with a single metallicity. This prescription for Galactic rate has previously been used by Dominik et al. (2013) and de Mink & Belczynski (2015).

For later use, we also estimate the rate of binary BH mergers which have two BHs in the mass ranges inferred for the progenitors of GW 150914. We do this by taking the number of mergers from the bin element used for Fig. 5 (see later) that the masses of the GW 150914 system lie in. This is all mergers with the masses of both BHs individually between 23.7 and 42.2 M$_\odot$.

We show our delay time distributions for sample metallicities in Fig. 2 for NS-NS, BH-NS and BH-BH mergers. The merger rates are present assuming an instantaneous burst of star formation at $t = 0$ with a total stellar mass of 10^6 M$_\odot$. We also indicate the delay

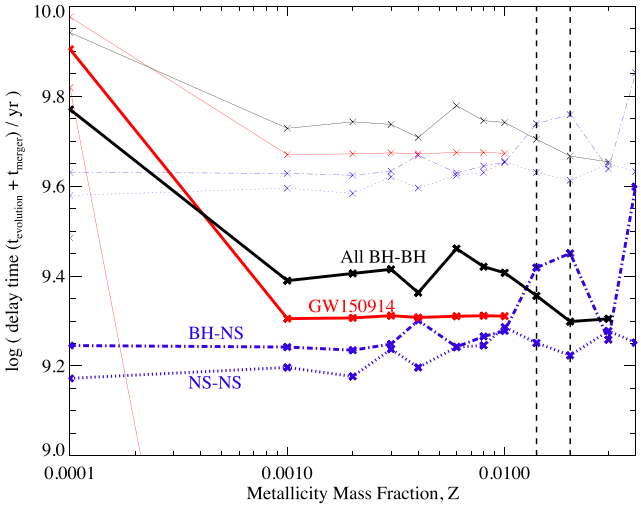

Figure 3. The mean total time to merge (i.e. $t_{\rm evolution} + t_{\rm Merger}$) as a function of metallicity. In all cases, the merger time dominates the delay time but the stellar lifetime does give rise to the minimum total time as shown in Fig. 2. The thick black line shows the mean time-scales for the full BH binary merger population with 1σ uncertainty indicated by the thin solid line. The red lines indicate the equivalent for systems with stellar masses matching those of GW 150914. Vertical lines indicate two widely used values for solar metallicity. The blue dotted lines are the merger times for NS-NS binaries and the dash–dotted the time for NS-BH mergers.

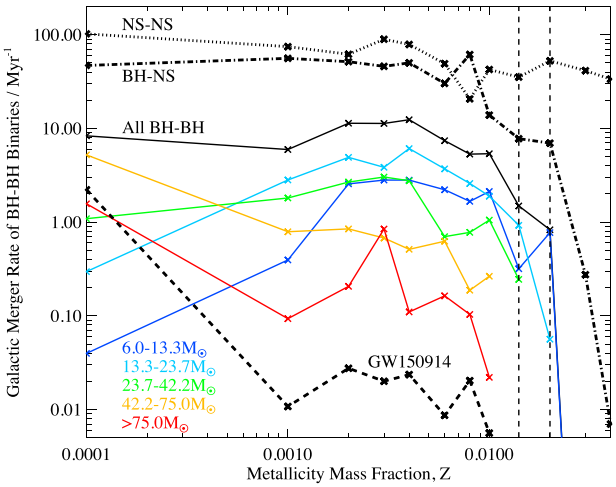

Figure 4. The Galactic merger rate of BH binaries, given a constant star formation rate of 3.5 $M_\odot$ yr^{-1} for 10 Gyr, as a function metallicity and the total mass of both BHs in the binary. The solid black line is the total Galactic rate of all the BH merger population, while the dashed black line is for systems matching GW 150914. The colour lines are the rates for logarithmically spaced mass bins of the mean BH mass in the binary with ranges ± 0.25 dex. Note the structure in metallicity behaviour. The dotted and dash–dotted lines are the rates for NS-NS and NS-BH binaries.

time distribution for GW 150914 type events. We see that for all distributions there are a short time-scale peak and a longer plateau. We discuss other aspects of the distribution below.

3 BINARY BH MERGER TIME-SCALES AND RATES

Fig. 3 presents the variation in the total lifetimes for mergers of binary BHs with metallicity. Our results are consistent with the results of Dominik et al. (2012) in that the typical delay times are a few Gyr although there is a broad range of possible merger times as shown in Fig. 2. We identify cases where the merger occurs after a much shorter delay due to the kick during the second core-collapse event reducing the orbital period or inducing a reasonable eccentricity that shortens the merger time. There are also cases with delay times longer than 10 Gyr but we do not include them in our rate estimate below, although we note that some authors (e.g. Belczynski et al. 2016a) include these. Delay times are relatively independent of initial stellar metallicity, although there is a slight trend to fewer mergers at higher metallicities. This is due to more mass-loss from the systems widening the orbit the progenitor binary systems as well as the reduction in the typical mass of the BHs.

At the lowest metallicities of $Z \leq 0.0001$, we see there is a trend for it to be more common for BHs to have longer merger times. The reduced opacities at this metallicity cause stars to be more compact and so we find common-envelope evolution is less likely and more mass can be transferred in binary interactions. This leads to more systems experiencing QHE with relatively wide orbits. When these form binary BH systems, most mass goes into the BH so such systems have low eccentricities and take a longer time to merge. We see, for example, that if the progenitor of GW 150914 had this metallicity it is most likely to have had a long merger time rather than being a prompt merger. We note that Belczynski et al. (2016a) also find the systems are dominated by long merger times at low metallicity and see similar evolution even without including any QHE in their models.

While the rate of mergers from these low-metallicity progenitors is higher than that at near-solar metallicities, the number of stars that formed at this metallicity is uncertain. We note that even by $z \sim 7$–8 there is strong evidence for much higher metallicities in the intergalactic medium (e.g. Kulkarni et al. 2013, and references therein) and above this redshift the cosmic star formation density history is very low (e.g. Madau & Dickinson 2014), so the fraction of the cosmic star formation history which takes place at such low metallicities is probably very small.

Fig. 4 and Table 1 demonstrate that our estimated Galactic merger rates (as defined in section 3) are more metallicity dependent than those reported by Dominik et al. (2012). The approximate range of rates are of the same order as those given by de Mink & Belczynski (2015). At supersolar metallicities the BH merger rate plummets: stellar mass-loss during the giant phase causes a decrease in the formation rate and typical mass of BH binaries and the systems are much wider at formation and fewer in number. The same trend can be seen in the neutron-star/BH binaries where the rate also decreases. Only the double NS merger rate remains relatively constant. We note that these rates are those derived for systems that merge within 10 Gyrs; it is likely that some systems at high metallicities may still merge, but on time-scales exceeding this cut-off.

Below solar metallicity, mass-loss becomes less efficient and our predicted binary BH merger rate increases slightly before plateauing at metallicities of $Z = 0.010$ and below. We also consider the relative rates in logarithmically spaced mass bins. The overall merger rate is dominated by binary systems with a total BH mass in the range 13–24 $M_\odot$. At lower metallicities, a slight increase in total rate is driven by a larger number of more massive systems (24–42 $M_\odot$), while the merger rate of less massive systems (6–14 $M_\odot$) declines. Very few BH systems with total mass of 100 $M_\odot$ are generated in our models, with small number statistics in each metallicity leading to variable rate estimates with a large associated uncertainty. These

Table 1. Fraction of mergers that arise due to QHE, for NS-NS, NS-BH, BH-BH and GW150914-like mergers. Also the Galactic merger rate for these same mergers and the typical eccentricities, e, initial BH-BH binary orbital separation, total BH binary mass and initial orbital separation for the BH-BH binaries.

	Fraction of QHE systems				Galactic merger rate/Myr^{-1}						
Z	NS-NS	BH-NS	BH-BH	GW150914	NS-NS	BH-NS	BH-BH	GW150914	e	$M_{\rm BHtot}$ ($M_\odot$)	log (P/d)
10^{-5}	0	0.061	0.878	0.989	160	29	3.1	0.14	0.34 ± 0.32	72 ± 49	0.7 ± 0.7
10^{-4}	0	0.008	0.858	0.988	100	47	8.3	2.2	0.24 ± 0.31	67 ± 36	0.7 ± 0.6
0.001	0	0.011	0.721	0.000	75	56	6.0	0.011	0.92 ± 0.16	28 ± 15	1.7 ± 0.9
0.002	0	0.023	0.692	0.000	62	52	11	0.028	0.91 ± 0.19	24 ± 19	1.5 ± 0.8
0.003	0.024	0.026	0.653	0.0002	89	46	11	0.021	0.86 ± 0.27	29 ± 29	1.4 ± 0.8
0.004	0.033	0.024	0.685	0.049	79	50	12	0.024	0.93 ± 0.14	21 ± 13	1.5 ± 0.8
0.006	0	0	0	0	49	30	7.4	0.009	0.84 ± 0.26	21 ± 16	1.2 ± 0.8
0.008	0	0	0	0	21	62	5.3	0.019	0.89 ± 0.16	21 ± 20	1.2 ± 0.9
0.010	0	0	0	0	43	14	5.4	0.006	0.87 ± 0.22	20 ± 12	1.4 ± 0.8
0.014	0	0	0	0	35	7.8	1.5	0	0.95 ± 0.11	17 ± 5	1.8 ± 0.7
0.020	0	0	0	0	52	7.0	0.82	0	0.98 ± 0.02	10 ± 2	1.6 ± 0.5
0.030	0	0	0	0	41	0.27	2×10^{-7}	0	0.9996 ± 0.0003	8	3.6 ± 0.1
0.040	0	0	0	0	34	0.007	0	0	0	0	0

represented a small contribution to the total rate at all but the lowest metallicities.

When QHE is included at $Z \leq 0.004$ there are changes to the rates. The main change is that at $Z = 0.004$ it causes the mean delay time to decrease by 0.1 dex, as seen in Fig. 3. Otherwise the mean BH delay time increases by 0.1 dex in our models over the range of metallicities while the other merger times remain mostly constant. We find this is due to our increasing BH mass giving rise to smaller natal kicks, giving rise to more circular BH binaries being formed. Less eccentric binaries have longer merger times giving rise to the shifting distribution. At our lowest metallicities $Z \leq 10^{-4}$ there is a significant increase of merger times of 0.5 dex. This is due to more of the mergers being dominated by QHE system which remain wider and therefore require more time to merge.

We note that an alternative approach is to discuss predictions in terms of event rate within the local Universe, per cubic Gpc per year. To obtain a meaningful estimate requires perfect knowledge of the luminosity function, star formation history, current star formation rate and metallicity distribution of galaxies in a given volume – all of which are subject to considerable uncertainties. However, it is possible to make an order of magnitude estimate for comparison with previous predictions. To do this we assume a number of Milky Way equivalent galaxies within a cubic Gpc of 0.01 Mpc^{-3} (see for example; Abadie et al. 2010). This can be combined with our rates of events per Myr in a Milky Way-like galaxy to produce a conversion factor of 1 Myr^{-1} (Galactic) $\approx$10 Gpc^{-3} yr^{-1} (volume averaged). Our predicted merger rates are, very approximately for all BH mergers, in the range of 10–100 Gpc^{-3} yr^{-1}. This is comparable to the merger rate inferred by Abbott et al. (2016e) of between 2 and 400 Gpc^{-3} yr^{-1}.

We note that in Fig. 4 our mergers of BH binaries with a total mass above 75 $M_\odot$ have a discontinuity between metallicities of $Z =$ 0.002 and 0.004. Below this metallicity jump, stars that previously would have formed BHs experience pair-instability SNe and so leave no remnant decreasing the rate of mergers from the most massive binaries. The rate increases again at the lowest metallicity with the increasing contribution from systems that experience QHE as well as now having more stars that are massive enough to avoid a pair-instability SNe and form very massive BHs. There is also similar non-monotonic variation with metallicity in some of the other merger rates. This is the result both of us using detailed models over a finite grid of masses and also that theoretical models suggest there is not a simple mapping between initial masses and remnant mass (Heger et al. 2003; Ugliano et al. 2012; Sukhbold et al. 2016), which also changes with metallicity (see fig. 6 in Eldridge & Tout 2004). There is some observational evidence for this from the fact that magnetars (highly magnetic neutron stars) arise from stellar progenitors with initial masses above 40 $M_\odot$ as well as lower mass progenitors of $\approx$17 $M_\odot$ (Belczynski & Taam 2008; Davies et al. 2009). These studies suggest that the final remnant masses are likely to be determined by mass-loss by winds and binary interactions but also the detailed nature of the final stages of nuclear burning.

The point to point variation in behaviour gives some indication of the uncertainties from our adopted methods, and are of the order of 0.3 dex at most. Our event rates for NS mergers, for example, is sensitive as well to the minimum mass for core-collapse SNe. This is 8 $M_\odot$ at $Z = 0.020$ but decreases to 6 $M_\odot$ at the lowest metallicities; at the same time the number of BHs forming is also changing and so the rate appears to jump.

In Table 1, we show the typical orbital parameters for the binary BH systems that merge in our simulations. We see that in general the systems require a high eccentricity to merge within 10 Gyr. This validates our earlier assumption of interpolating between the limits of high and low eccentricity derived by Peters (1964) as most systems are highly eccentric after the second SN. Furthermore, we note again that at the lowest metallicities there is a significant decrease in the mean eccentricity. This is due to the fact that at lower metallicities, the QHE stars are significantly more compact at the end of the evolution and eject very little mass in the second SN. Therefore the orbit remains relatively circular and so the merger time remains high.

We see a similar pattern for the typical system giving rise to events matching GW150914 in Table 2, although due to the restriction of the masses we find that at higher metallicities the possible systems are very few. At lower metallicities, there are two ranges of initial masses due to pair-instability SNe preventing stars from forming BHs at some mass ranges. Again we see that most of our systems are required to have high initial eccentric when formed, unless the systems are at the lowest metallicities when QHE is the dominant formation channel – although as we see in Fig. 2 these have long merger times. Since these would have formed earlier in the Universe at these metallicities, it is possible that this is a likely formation channel for GW 150914, although as we discuss above few stars were formed at low metallicities.

Table 2. The parameters of systems that would result in GW 150914-like progenitor binaries. We show mass ranges and typical initial periods for the stars at different phases of the binary progenitors lifetime. $M_{1,i}$, $M_{2,i}$ and $\log(P_{i,1}/\mathrm{d})$ are the initial masses and periods of the binary stars. $M_{1,\mathrm{BH}}$, $M_{2,p\mathrm{SN}}$ and $\log(P_{i,2}/\mathrm{d})$ are the typical mass of the BH from the first SN, effective secondary mass range, including results of mass transfer and typical period post-SN. Finally, $M_{1,\mathrm{BH}}$ and $M_{2,\mathrm{BH}}$ are the final masses of the BHs formed, we also show typical eccentricities, e, total BH binary mass and initial orbital separation for the BH-BH binaries.

Z	$M_{1,i}$ ($\mathrm{M}_\odot$)	$M_{2,i}$ ($\mathrm{M}_\odot$)	$\log(P_{i,1}$ /d)	$M_{1,\mathrm{BH}}$ ($\mathrm{M}_\odot$)	$M_{2,\mathrm{pSN}}$ ($\mathrm{M}_\odot$)	$\log(P_{i,2}$ /d)	$M_{1,\mathrm{BH}}$ ($\mathrm{M}_\odot$)	$M_{2,\mathrm{BH}}$ ($\mathrm{M}_\odot$)	e	M_{BHtot} ($\mathrm{M}_\odot$)	$\log(P/\mathrm{d})$
10^{-5}	40–80, 100	20–90	≥0	25–40	35–100	0.6–0.8, ≥3.8	20–40	27–40	0.05 ± 0.08	79 ± 4	0.7 ± 0.2
10^{-4}	60–80, 120	24–65	≥0.6	25–40	40–70	≥3.6	25–40	24–40	0.07 ± 0.06	69 ± 6	0.6 ± 0.2
0.001	80, 100	40–72	≥0.6	32–40	70–100	≥3.6	32–41	28–41	0.9994 ± 0.0006	67 ± 6	4.0 ± 0.3
0.002	120	40–110	≥0.8	32–40	70–100	≥3.2	25–41	25–35	0.9994 ± 0.0006	64 ± 6	4.0 ± 0.3
0.003	100–200, 300	60–180	≥0.8	32–40	80–100	≥3.4	32–40	24–31	0.9993 ± 0.0006	63 ± 6	4.0 ± 0.4
0.004	120–200, 300	75–180	≥1	25–40	100–120	≥3.2	25–40	27–38	0.9994 ± 0.0006	62 ± 7	4.1 ± 0.4
0.006	100–300	70–150	≥0	32–40	120–150	≥3.4	25–40	24–41	0.9994 ± 0.0007	68 ± 9	4.1 ± 0.5
0.008	200	180	≥1.4	25–32	120–200	≥2.4	25–34	26–37	0.9994 ± 0.0007	57 ± 6	4.1 ± 0.5
0.010	200	120	1.2	16–25	120	≥2	25–40	25	0.9991 ± 0.0008	50 ± 1	3.8 ± 0.4

Table 3. Mean chirp masses for different types of compact remnant mergers and the approximate relative detection rate this implies relative to the mean rate of NS-NS mergers. This is calculated by assuming the volume within which mergers can be detected is given by $\mathcal{M}_0^{5/2}$, the mean rate of NS-NS mergers is then calculated as the mean of all the metallicities considered.

	Mean chirp mass, $\mathcal{M}_0$			Relative detection rate		
Z	NS-NS	BH-NS	BH-BH	NS-NS	BH-NS	BH-BH
10^{-5}	1.22	3.08 ± 1.04	27.3 ± 18.1	2.44	4.52	115
10^{-3}	1.22	3.15 ± 0.93	25.5 ± 12.9	1.58	7.80	258
0.001	1.22	3.06 ± 0.86	9.47 ± 4.40	1.16	8.64	15.5
0.002	1.22	2.93 ± 0.82	8.77 ± 7.18	0.96	7.13	24.5
0.003	1.22	2.88 ± 0.72	10.9 ± 11.3	1.38	6.10	42.1
0.004	1.22	2.66 ± 0.63	7.79 ± 4.30	1.22	5.48	19.9
0.006	1.22	2.61 ± 0.61	8.07 ± 5.64	0.76	3.13	12.9
0.008	1.22	3.99 ± 1.79	7.18 ± 3.64	0.32	18.4	6.94
0.01	1.22	2.54 ± 0.61	7.21 ± 3.42	0.66	1.35	7.07
0.014	1.22	2.55 ± 0.96	6.45 ± 1.60	0.55	0.77	1.49
0.02	1.22	2.14 ± 0.41	4.07 ± 0.68	0.81	0.44	0.26
0.03	1.22	2.52 ± 0.47	3.29 ± 0.00	0.64	0.03	5×10^{-8}
0.04	1.22	1.87 ± 0.10	0.00 ± 0.00	0.52	0.0003	–
Mean	1.22	2.8	11	1	4.9	42

Finally, we provide a very approximate estimate of how detectable the different mergers will be in Table 3. For each metallicity, we calculate the mean chirp masses for all our compact remnant mergers in our calculations where, $\mathcal{M}_0 = (M_1 M_2)^{3/5}/(M_1 + M_2)^{1/5}$. The distance at which a merger can be detected is related to this value by $d \propto \mathcal{M}_0^{5/6}$, the volume within which mergers can be detected is thus $\propto \mathcal{M}_0^{5/2}$. Rather than calculate an absolute rate, we calculate the rates relative to the mean merger rate for all NS-NS mergers. We see that, except at the lowest metallicity, the NS-NS merger rates are similar. However with the higher chirp masses for systems involving a BH our approximate detection rate increase significantly. This echoes the predictions of (Belczynski et al. 2010; Dominik et al. 2015) that a binary BH would be the first remnant mergers to be detected.

4 EFFECTS OF BH-BH MASS RATIO

As Fig. 5 illustrates, the rate of mergers at $Z \geq 0.004$ peaks in systems where the primary BH is just over twice that of the secondary (a mass ratio of 2), and is highest for primary BHs around 10 $\mathrm{M}_\odot$. Comparable rates (to within an order of magnitude) are found for some binaries with mass ratios ranging from 10 to 0.5, although this is dependent on both metallicity and primary mass. At metallicities close to solar, BH binaries with masses >30 $\mathrm{M}_\odot$ (in either the secondary or primary) are rarely seen in our models. At lower metallicities ($Z < 0.004$), the structure in rates becomes more complex, with the highest rates observed or systems in which the primary is still close to 10 $\mathrm{M}_\odot$ in mass but now comparable to, or even *less* massive than, the secondary, although several regions of parameter space with a range of mass ratios and primary masses show comparable rates. At the lowest metallicities, we show ($Z = 10^{-4}$), the rate distribution of mergers is predicted to show two peaks of comparable strength, one of which occurs at near-equal masses comparable to those of GW 150914, while the other occurs at lower masses and more asymmetric systems.

There are two competing pathways for the BH mergers in our synthetic population. The first is for systems that do not require QHE. These are interacting massive binary systems driven together by common-envelope evolution or wider binary systems that only experience Roche lobe overflow and require a more eccentric BH binary to merge quickly. For these systems typically the primary BH is the more massive one. Systems with a more massive secondary BH

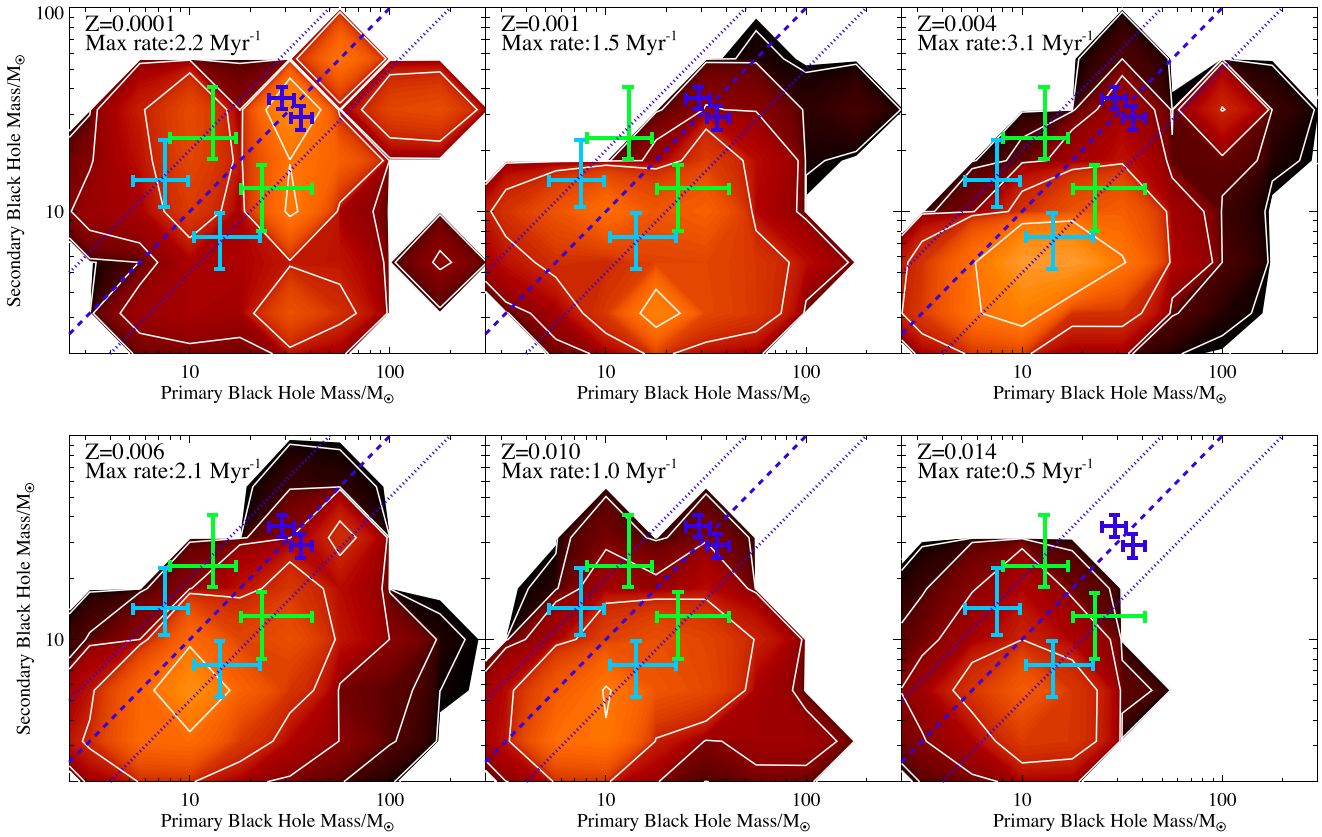

Figure 5. The dependence of binary BH Galactic merger rate on BH mass and mass ratio. The coloured contours represent the relative rates. The white contours are lines of constant merger rate for every order of magnitude, i.e. 1, 0.1, 0.01, 10^{-3} and 10^{-4} Myr^{-1} for a population forming stars at a constant rate of 3.5 $\mathrm{M}_{\odot}$ yr^{-1} over a 10 Gyr period, we note in the $Z = 0.014$ panel the maximum rate is too low for the first contour to be included. Blue crosses (the crosses with the highest masses towards the upper right of the panels) represent the inferred masses of the BHs in GW 150914 and their uncertainties. The two points indicate different evolutionary behaviour dependent on whether the more massive BH was formed first or second. The dashed line represents a BH mass ratio of unity, while the dotted lines represent scenarios in which one BH is twice the mass of the other. We also indicate the progenitor masses of the recently announced events GW 151226 and LVT 151012 (Abbott et al. 2016f, see section 6) in light blue and green (the crosses towards the lower left and in the middle on the panels), respectively.

are less probable. For this pathway decreasing metallicity increases the typical BH masses slightly.

The second is an interaction leading to efficient mass transfer so that the secondary star can accrete a large amount of material and at low metallicities experience QHE. At $Z = 0.004$, the peak from this pathway overlaps with that from the typical mass transfer. However as the metallicity decreases the secondary star retains more of its mass as stellar winds weaken and so the peak of events switches to the secondary BH being more massive. We show in Table 1 the fraction of mergers at each metallicity that arise from systems that have experienced QHE. We see that this is a major channel for most BH-BH mergers but, in agreement with Belczynski et al. (2016a) we find that GW 150914 is possible and more likely from interacting binary evolution without QHE, except at the lowest metallicities we consider.

One difference between the standard and QHE pathways is that the QHE pathway tends to have a longer delay time. In the standard binary pathway both stars can interact, so when the second BH is formed the stars can already be in a tight orbit. For the QHE pathway, the lack of a second interaction leads to wider orbits and therefore longer merger times. The extreme case of this can be seen in the $Z = 0.0001$ delay time panel of Fig. 2 with the peak around 10 Gyr.

A final factor to consider is how many of our BH mergers are predicted to have a mass ratio close to unity. From summing the bins with mass ratio consistent with the unity line in Fig. 5, we find that at $Z \geq 0.001$ approximately 20–40 per cent of BH mergers should have similar BH masses. At metallicities below this value, the number can drop to a less than 10 per cent because of the QHE stars dominating the rate.

We note that this occurs in our observationally benchmarked standard model set, in the absence of fine tuning to match the GW 150914 event. The observational benchmarking of BPASS has previously concentrated on modelling observed stars, stellar systems and core-collapse SNe. This is the first time we have confronted predictions for compact remnants. GW150914 has provided a new test of BPASS that other spectral synthesis codes such as STARBURST99 (Leitherer et al. 1999) and the Bruzual & Charlot (2003) models are unable to pass due to their reliance on single-star models.

5 IMPLICATIONS FOR ELECTROMAGNETIC FOLLOW-UP

While a low significance gamma-ray burst transient coincident with the GW 150914 event was reported by Connaughton et al. (2016), the association of this with the binary inspiral and merger is unclear. In a separate analysis Greiner et al. (2016) found this signal was consistent with background fluctuations. Follow up with other instrumentation ranging from radio to X-ray wavelengths (Abbott

et al. 2016d) failed to yield a detection. Such an identification was always unlikely given the low luminosities predicted for BH-BH merger counterparts, the poor sky localization of LIGO in its 2015 configuration, and the early detection at a time when a number of the planned electromagnetic follow-up programmes (e.g. BlackGEM; Bloemen et al. 2015, or GOTO, http://goto-observatory.org/) were not yet on sky. BH-BH mergers are considered poor candidates for electromagnetic detection, but this is yet to be demonstrated observationally. As such, it is useful to consider the implications of our analysis for hypothetical follow-up of similar future events.

LIGO in its current configuration (two detectors in the United States), can localize events to a region of the order of ∼500–1000 deg^2, with this region typically distributed in an arc with multiple high probability regions rather than a single field (Singer et al. 2014; Essick et al. 2015). Identification of counterparts in such large regions is exceptionally difficult due both to the small field of view of typical optical telescopes and the number of 'normal' electromagnetic transients expected per square degree. Suggested follow-up strategies include optimised tiling of the highest probability regions (e.g. Ghosh et al. 2016) and targeting the environs of the brightest galaxies in the region (which contribute ∼50 per cent of the stellar light, e.g. White, Daw & Dhillon 2011; Gehrels et al. 2015). While the former strategy is unaffected by our results, the effect on the latter could be significant. Galaxy catalogues compiled to date have been based on a distance range and luminosity cut-off optimized for NS-NS mergers, and tuned to select the typical host galaxies of short GRBs (e.g. Gehrels et al. 2015). They prioritize galaxies on B-band luminosity, focusing on the large-scale structures containing most luminous mass. Given the strong metallicity dependence of our results, using such catalogues may not be an optimal strategy for binary BH mergers.

As discussed in Section 3, we see two peaks in the age distribution of GW 150914-like progenitors at the lowest metallicities we consider arising from different pathways. The first of these allows systems to merge at ages of a few million years, while the second dominates at ages of a few billion years upwards. At any metallicity in our models above $Z = 0.0001$, only the first of these pathways is permitted.

While it is appealing to abandon the short-lived possibility in favour of the longer lived progenitor pathway, there are potential problems. The rate expected from long-lived progenitors in our models peaks at 10 Gyr and is only measurable at metallicities below a 200th of Solar. In this scenario the stars that ended their lives in GW 150914 likely formed at $z \sim 2$, and at metallicities significantly lower than those estimated in the star-forming galaxy population at that redshift (e.g. Turner et al. 2014). They would have to arise in pockets of pristine or near-pristine gas isolated from pollution by nearby SNe – very rare survivors of the metal-poor cosmic dawn. While it is possible to push the formation redshift still earlier (i.e. invoking merger time-scales >10 Gyr), we note that the star formation density at such early times falls off rapidly was many orders of magnitude lower at an epoch when the required metallicities were common (see Madau & Dickinson 2014, for discussion).

On the other hand, the short-lived progenitor pathway also requires that the stars that ended their lives in GW 150914 formed in a gas cloud that is significantly below the volume averaged typical metallicity at its redshift. One advantage is that such short-merger systems form at a wide range of more moderate metallicities. At any metallicity above $Z = 0.001$, and given the event redshift, $z \sim 0.049$, the stars that ended their lives in GW 150914 likely formed at $z \leq 0.4$, while more typical BH-BH merger progenitors formed at $z \sim 0.5$, an epoch at which the Universe was already heavily metal enriched. However galaxies with metallicities below half-Solar (required by our models) are not unknown in the local Universe (see e.g. James et al. 2013), although their number density is low and remains poorly constrained.

Galaxies in the local Universe show a strong relation between metallicity and both stellar mass and luminosity, with bright ($M_g \lesssim -19$), massive ($M_* \gtrsim 10^{10}\,M_\odot$) galaxies typically having solar or supersolar metallicities (Tremonti et al. 2004). While there are likely to be pockets of lower metallicity star formation in these systems, the bulk properties mitigate against the formation of high mass BH-BH binaries. Instead, short-time-scale binary BH merger events are more likely to be associated with low mass, less luminous regions of the cosmic web and potentially with post-starburst galaxies (i.e. those which formed significant numbers of stars ∼3–5 Gyr ago). Hence, even if galaxy catalogues were extended to the larger distances expected for BH-BH mergers relative to NS-NS mergers, their analysis of the densest regions of stellar material may still skew observations away from the best candidates.

While we have not investigated NS-BH events in detail, we expect them to exhibit a similar bias towards low metallicities – whether formed through short or long time-scale pathways. We advocate the addition of galaxy metallicity information to follow-up prioritization algorithms using galaxy catalogues. These should be employed with care, particularly if the LIGO rapid analysis is able to constrain an event as a likely binary BH merger before electromagnetic follow-up.

6 CONCLUSIONS

We can conclude that the most likely evolutionary pathway for GW 150914 is standard binary evolution, in agreement with the work of Belczynski et al. (2016a), who independently reached the same conclusion. Having said that, there are differences between these two population synthesis codes regarding handling of core collapse and the natal kicks of neutron stars and BHs. This leads to our predictions giving wider BH binaries that are highly eccentric and merge within 10 Gyr, while Belczynski et al. (2016a) have shorter period systems that undergo direct BH formation.

As more compact remnant mergers are detected there will be ever tighter constraints on binary population synthesis. However, we stress this should only be one test and other observational data such as stellar populations and SNe should be used to constrain population synthesis codes. The results presented in this paper are based on v2.0 of the BPASS models, which have already been tested against observational constraints in a range of different areas from the distant Universe to local star-forming galaxies (e.g. Ma et al. 2016; Stanway et al. 2016; Wofford et al. 2016, and references therein). Inevitably, their results are somewhat dependent on the initial parameter distributions employed by the models (for example in binary separation distribution and mass-loss rates), and we endeavour to use observationally motivated constraints for all free parameters. Importantly, however, we have not tuned our models to achieve the results in this paper. We have simply taken the standard BPASS model set and analysed its predictions for BH mergers.

We have calculated predictions for binary BH merger time-scales and rates, and considered the first LIGO event detection in light of these predictions. We find that the event must have come from a metallicity of $Z = 0.010$, roughly half-Solar, or below and the rate for such events is nearly constant for metallicities between 1/5th and 1/10th Solar via normally binary evolution at 0.1–0.4 per cent of all binary BH mergers. This metallicity cut-off was estimated independently by Abbott et al. (2016c) using the single-star models

of Spera et al. (2015). However both these cut-offs are higher than the metallicity cut-off given by the binary population synthesis of Belczynski et al. (2016a) of 1/10th Solar or $Z = 0.002$. The exact reason for this difference is not clear and it is likely to be a combination of factors:

(i) We may estimate more massive BHs in our simulations, either due to our method of estimating the remnant mass formed or our assumed stellar-wind mass-loss scheme or other model detail. However as shown in Fig. 1 our estimated BH masses are not so high, and are consistent with observations of known Galactic systems. If we were to change the physics to decrease the BH masses then the observed BH masses in nearby stellar binaries would become extreme rather than typical systems.

(ii) Our BH kick model may be weak compared to others. We pick a kick at random from a Maxwell–Boltzmann distribution with $\sigma = 265\,\mathrm{km\,s^{-1}}$ (Hobbs et al. 2005), but using it as a momentum distribution for the BHs so that the kick velocity is reduced by $M_{\rm BH}/(1.4\,\mathrm{M_{\odot}})$. This means more massive BHs are likely to have weaker kicks and remain bound (see the blue line in Fig. 1). This means more low-mass BHs will be runaway compact remnants and are more likely to be detected by gravitational microlensing (e.g. Wyrzykowski et al. 2016).

(iii) The detail of our treatment of common-envelope evolution could also produce more BH binaries. While many groups include common-envelope evolution it is the most uncertain phase of an interacting binary system (Ivanova et al. 2013).

The differences between the different model populations are essentially linked to the formation of BHs, both in how massive they can be upon formation and what kick they obtain in their birth. Future gravitational wave events will provide unique insights into the final outcome of core-collapse SNe and the formation of BHs.

Comparing our maximum BH masses to those presented in Belczynski et al. (2016a), we find the difference between predicted BH masses is roughly a factor between 1.25 and 2 at metallicities around Solar and below. The assumed method of calculating remnant masses from the final stellar model likely contributes to this, as does our use of detailed evolution models rather than the rapid models. While in general rapid models are sufficiently accurate to estimate the evolution of a star, in the cases of significant mass-loss the results can differ to those from detailed models. For example, in cases where the hydrogen envelope of a massive star is close to being removed a detailed model will end its evolution as a yellow supergiant, while a rapid model typically predicts the star becomes a Wolf–Rayet star. In such cases, the eventual mass of the star and compact remnant will be different. In addition, as discussed above, binary interactions can lead to a star forming a more massive BH than it would in single-star evolution. These are only second-order effects and can be accounted for in rapid models to some degree but can only be revealed by a detailed evolution model due to the highly non-linear nature of stellar evolution.

We note that Marchant et al. (2016) also used a grid of detailed evolution models to investigate the evolution of binary stars in tight orbits that experience QHE driven by tides rather than mass transfer. They also find a metallicity cut-off similar to that of Belczynski et al. (2016a). However they did not investigate the standard binary evolution channel that is presented here and that metallicity limit is for the massive overcontact binary pathway when the two stars are tidally locked and both experience QHE. We do not include this pathway in our study.

For a very low metallicity ($Z \leq 10^{-4}$), 1/200th Solar, the merger rates predicted by BPASS are at their highest, a factor of 100 greater than at higher metallicities. For a stellar population undergoing constant star formation, the rate of binary BH merger events in our models peaks at close to the mass of the BHs inferred for GW 150914. However at more typical stellar metallicities, this event would constitute a less common high-mass outlier in the predicted distribution. The predictions of BPASS are consistent with this event arising from a normal, if low metallicity, stellar population. While other scenarios, such as that suggested by Mandel & de Mink (2016) and Marchant et al. (2016), could also lead to the formation of such a binary, exotic scenarios are not necessarily required. We note the importance of considering metallicity biases in the host stellar population when attempting to localise electromagnetic counterparts for binary merger events.

Finally, while this paper has been under review the LIGO consortium have announced the detection of a further binary BH merger, and undertaken further analysis of a third, low significance event (Abbott et al. 2016f). Neither event had a detected optical counterpart. We have included these events (GW 151226 and LVT 151012) on Fig. 5. Their total BH binary masses of 37 and 22 $\mathrm{M_{\odot}}$ are lower than that of GW150914 and, as we can see in Fig. 4, rates of similar events are expected to be higher and more typical of what is expected from binary BH mergers in the Universe. We note with interest that one or both of the two BHs in GW 151226 may have had intrinsic spin. As the population of gravitational wave events grows, this signal will be key to identifying cases where QHE is important in producing the progenitor system. Together the three events have also allowed the LIGO consortium to report a more accurate estimate for the expected merger rate of 9–240 $\mathrm{Gpc^{-3}\,yr^{-1}}$ (Abbott et al. 2016f), comparable to the estimate presented in this work of 10–100 $\mathrm{Gpc^{-3}\,yr^{-1}}$.

ACKNOWLEDGEMENTS

JJE acknowledges support from the University of Auckland. ERS acknowledges support from UK STFC consolidated grant ST/L000733/1. We thank Richard Easther for useful discussion. We acknowledge and thank the LIGO Scientific Collaboration for their decades of endeavours that led to the detection of GW150914. We wish to acknowledge the contribution of the NeSI high-performance computing facilities and the staff at the Centre for eResearch at the University of Auckland. New Zealand's national facilities are provided by the New Zealand eScience Infrastructure (NeSI) and funded jointly by NeSI's collaborator institutions and through the Ministry of Business, Innovation and Employment Infrastructure programme (http://www.nesi.org.nz).

REFERENCES

Abadie J. et al., 2010, Class. Quantum Gravity, 27, 3001
Abbott B. P. et al., 2016a, Phys. Rev. Lett., 116, 061102
Abbott B. P. et al., 2016b, Phys. Rev. Lett., 116, 241102
Abbott B. P. et al., 2016c, ApJ, 818, L22
Abbott B. P. et al., 2016d, 826, L13
Abbott B. P. et al., 2016e, preprint (arXiv:1602.03842)
Abbott B. P. et al., 2016f, preprint (arXiv:1606.04856)
Allende Prieto C., Lambert D. L., Asplund M., 2002, ApJ, 573, L137
Asplund M., 2005, ARA&A, 43, 481
Belczynski K., Taam R. E., 2008, ApJ, 685, 400
Belczynski K., Dominik M., Bulik T., O'Shaughnessy R., Fryer C., Holz D. E., 2010, ApJ, 715, L138
Belczynski K., Wiktorowicz G., Fryer C. L., Holz D. E., Kalogera V., 2012, ApJ, 757, 91

Belczynski K., Holz D. E., Bulik T., O'Shaughnessy R., 2016a, Nature, 534, 512
Belczynski K., Repetto S., Holz D., O'Shaughnessy R., Bulik T., Berti E., Fryer C., Dominik M., 2016b, ApJ, 819, 108
Berry C. P. L. et al., 2015, ApJ, 804, 114
Bloemen S., Groot P., Nelemans G., Klein-Wolt M., 2015, in Rucinski S M., Torres G., Zejda M., eds, ASP Conf. Ser. Vol. 496, Living Together: Planets, Host Stars and Binaries. Astron. Soc. Pac., San Francisco, p. 254
Bobrick A., Davies M. B., Church R. P., 2015, in Rosquist K. et al., eds, Proc. MG13 Meeting on General Relativity: On Recent Developments in Theoretical and Experimental General Relativity, Astrophysics and Relativistic Field Theories. World Scientific Press, Singapore, p. 1820
Bogomazov A. I., Lipunov V. M., Tutukov A. V., 2007, Astron. Rep., 51, 308
Bruzual G., Charlot S., 2003, MNRAS, 344, 1000
Carr B. J., 2003, in Giulini D., Kiefer C., Lämmerzahl C., eds, Lecture Notes in Physics, Vol. 631, Quantum Gravity: From Theory to Experimental Search. Springer-Verlag, Berlin, p. 301
Connaughton V. et al., 2016, ApJ, 826, L6
Crowther P. A., Barnard R., Carpano S., Clark J. S., Dhillon V. S., Pollock A. M. T., 2010, MNRAS, 403L, 41
Davies B., Figer D. F., Kudritzki R.-P., Trombley C., Kouveliotou C., Wachter S., 2009, ApJ, 707, 844
de Mink S. E., Belczynski K., 2015, ApJ, 814, 58
Dominik M., Belczynski K., Fryer C., Holz D. E., Berti E., Bulik T., Mandel I., O'Shaughnessy R., 2012, ApJ, 759, 52
Dominik M., Belczynski K., Fryer C., Holz D. E., Berti E., Bulik T., Mandel I., O'Shaughnessy R., 2013, ApJ, 779, 72
Dominik M. et al., 2015, ApJ, 806, 263
Dosopoulou F., Kalogera V., 2016a, ApJ, 825, 70
Dosopoulou F., Kalogera V., 2016b, ApJ, 825, 71
Eldridge J. J., 2009, MNRAS, 400, 20
Eldridge J. J., Stanway E. R., 2009, MNRAS, 400, 1019
Eldridge J. J., Stanway E. R., 2012, MNRAS, 419, 479
Eldridge J. J., Tout C. A., 2004, MNRAS, 353, 87
Eldridge J. J., Izzard R. G., Tout C. A., 2008, MNRAS, 384, 1109
Eldridge J. J., Langer N., Tout C. A., 2011, MNRAS, 414, 3501
Eldridge J. J., Fraser M., Smartt S. J., Maund J. R., Crockett R. M., 2013, MNRAS, 436, 774
Eldridge J. J., Fraser M., Maund J. R., Smartt S. J., 2015, MNRAS, 446, 2689
Essick R., Vitale S., Katsavounidis E., Vedovato G., Klimenko S., 2015, ApJ, 800, 81
Gehrels N., Cannizzo J. K., Kanner J., Kasliwal M. M., Nissanke S., Singer L. P., 2015, ApJ, 820, 136
Ghosh S., Bloemen S., Nelemans G., Groot P. J., Price L. R., 2016, A&A, 592, 82
Greiner J., Burgess J. M., Savchenko V., Yu H.-F., 2016, ApJ, in press
Heger A., Woosley S. E., 2002, ApJ, 567, 532
Heger A., Fryer C. L., Woosley S. E., Langer N., Hartmann D. H., 2003, ApJ, 591, 288
Hobbs G., Lorimer D. R., Lyne A. G., Kramer M., 2005, MNRAS, 360, 974
Hulse R. A., Taylor J. H., 1975, ApJ, 195, L51
Hurley J. R., Tout C. A., Pols O. R., 2002, MNRAS, 329, 897
Ivanova N. et al., 2013, A&AR, 21, 59
Izzard R. G., Ramirez-Ruiz E., Tout C. A., 2004, MNRAS, 348, 1215
James B. L., Tsamis Y. G., Walsh J. R., Barlow M. J., Westmoquette M. S., 2013, MNRAS, 430, 2097
Kiminki D. C., Kobulnicky H. A., 2012, ApJ, 751, 4
Kowalska-Leszczynska I., Regimbau T., Bulik T., Dominik M., Belczynski K., 2015, A&A, 574, A58
Kroupa P., Tout C. A., Gilmore G., 1993, MNRAS, 262, 545
Kulkarni G., Rollinde E., Hennawi J. F., Vangioni E., 2013, ApJ, 772, 93
Leitherer C. et al., 1999, ApJS, 123, 3
LIGO Scientific Collaboration et al., 2015, Class. Quantum Gravity, 32, 074001
Lipunov V. M., Pruzhinskaya M. V., 2014, MNRAS, 440, 1193
Ma X., Hopkins P. F., Kasen D., Quataert E., Faucher-Giguere C.-A., Keres D., Murray N., Strom A., 2016, MNRAS, 459, 3614
Madau P., Dickinson M., 2014, ARA&A, 52, 415
Mandel I., 2016, MNRAS, 456, 578
Mandel I., de Mink S. E., 2016, MNRAS, 458, 2634
Marchant P., Langer N., Podsiadlowski P., Tauris T. M., Moriya T. J., 2016, A&A, 588A, 50
Mennekens N., Vanbeveren D., 2016, A&A, 589, A64
Nieva M.-F., Przybilla N., 2012, A&A, 539A, 143
Özel F., Psaltis D., Narayan R., McClintock J. E., 2010, ApJ, 725, 1918
Peters P. C., 1964, Phys. Rev., 136, 1224
Podsiadlowski P., 1992, PASP, 104, 717
Sana H. et al., 2012, Science, 337, 444
Sana H. et al., 2014, ApJS, 215, 15
Singer L. P. et al., 2014, ApJ, 795, 105
Spera M., Mapelli M., Bressan A., 2015, MNRAS, 451, 4086
Stanway E. R., Eldridge J. J., Greis S. M. L., Davies L. J. M., Wilkins S. M., Bremer M. N., 2014, MNRAS, 444, 3466
Stanway E. R., Eldridge J. J., Becker G. D., 2016, MNRAS, 456, 485
Sukhbold T., Ertl T., Woosley S. E.., Brown J. M., Janka H.-T., 2016, ApJ, 821, 38
Tinsley B. M., Gunn J. E., 1976, ApJ, 203, 52
Tremonti C. A. et al., 2004, ApJ, 613, 898
Turner M. L., Schaye J., Steidel C. C., Rudie G. C., Strom A. L., 2014, MNRAS, 445, 794
Tutukov A., Yungelson L., 1973, Nauchn. Inf., 27, 70
Ugliano M., Janka H.-T., Marek A., Arcones A., 2012, ApJ, 757, 69
Vanbeveren D., De Loore C., Van Rensbergen W., 1998, A&AR, 9, 63
Villante F. L., Serenelli A. M., Delahaye F., Pinsonneault M. H., 2014, ApJ, 787, 13
Vink J. S., de Koter A., Lamers H. J. G. L. M., 2001, A&A, 369, 574
Walborn N. R., Lasker B. M., Laidler V. G., Chu Y.-H., 1987, ApJ, 321, L41
White D. J., Daw E. J., Dhillon V. S., 2011, Class. Quantum Gravity, 28, 085016
Wiktorowicz G., Sobolewska M., Sadowski A., Belczynski K., 2015, ApJ, 810, 20
Wilkins S. M., Feng Y., Di Matteo T., Croft R., Stanway E. R., Bouwens R. J., Thomas P., 2016, MNRAS, 458, L6
Wofford A. et al., 2016, MNRAS, 457, 4296
Wyrzykowski L. et al., 2016, MNRAS, 458, 3012
Xiao L., Eldridge J. J., 2015, MNRAS, 452, 2597
Yoon S.-C., Langer N., Norman C., 2006, A&A, 460, 199
Yusof N. et al., 2013, MNRAS, 433, 1114

This paper has been typeset from a TEX/LATEX file prepared by the author.